

Supporting Information © Wiley-VCH 2010

69451 Weinheim, Germany

Transition-Metal-Promoted Chemoselective Photoreactions at the Cucurbituril Rim**

Apurba L. Koner, Cesar Márquez, Michael H. Dickman, and Werner M. Nau*

anie_201005317_sm_miscellaneous_information.pdf

Experimental Section. The azoalkanes DBH and DBO^[1-5] as well as cucurbit[7]uril^[6-8] were synthesized as reported. All metal salts were purchased as chlorides, sulfates (only Tl⁺), or nitrates (only for Ag⁺, Cr³⁺, Cd²⁺, and Pb²⁺) from Fluka. Cadaverine (1,5-diaminopentane), GC-quality organic solvents, as well as the GC standards cyclopentene and 1,5-hexadiene were from Sigma-Aldrich. UV spectra were recorded on a Varian Cary 4000, ¹H NMR spectra on a Jeol JNM-ECX400, and fluorescence spectra on a Varian Cary Eclipse fluorometer. All measurements were performed in millipore water by adjusting their pH, where necessary, to pH 5 with a WTW 330i pH meter equipped with a WTW SenTix Mic glass electrode. The pD of the D₂O solutions was accordingly adjusted to pD 5.4.

Spectrophotometric evidence for the formation of the binary complexes

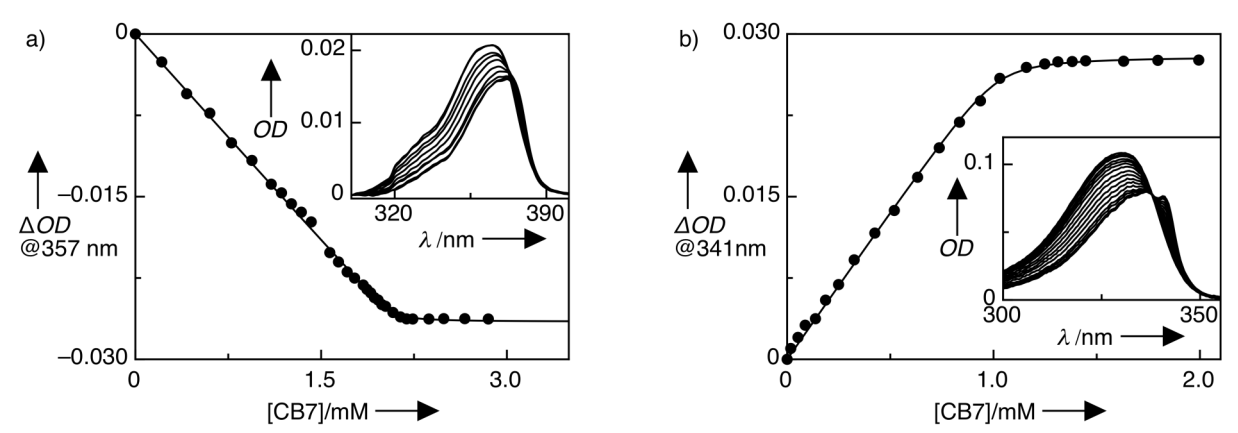


Figure S1. Variation in the UV spectra (insets) and corresponding titration plots of a) 2.0 mM DBO (inset: 0.4 mM) and b) 1.0 mM DBH upon addition of increasing amounts of CB7 at pH 5.0. The data were fitted according to a 1:1 complexation model and provided lower limits of the binding constants as $> 10^6$ M⁻¹ for DBO and $> 10^5$ M⁻¹ for DBH. Subsequent isothermal calorimetric titrations at lower concentrations afforded values of $(5.8 \pm 0.2) \times 10^6$ M⁻¹ for DBO and $(3.8 \pm 0.2) \times 10^5$ M⁻¹ for DBH.

NMR spectroscopic evidence for the formation of binary and ternary complexes

Table S1. Complexation-induced chemical shifts of the DBO protons upon addition of CB7 (binary complex) and Ag⁺ (metal-ligand complex) and upon addition of both additives (ternary complex) in D₂O at pD 5.4

		∂/ppm		
System	H_{endo}	H_{exo}	H_b	$\Delta \delta_{ m avg}/{ m ppm}$
DBO	1.11	1.56	5.01	= 0.00
$DBO \bullet Ag^{+ [a]}$	1.33	1.69	5.16	+0.17
DBO•CB7 [b]	0.33	0.74	[d]	-0.80
DBO•CB7•Ag ^{+ [c]}	0.45	0.90	[d]	-0.66

[[]a] 1.0 mM DBO, 25.0 mM Ag⁺. [b] 1.0 mM DBO, 1.5 mM CB7. [c] 1.0 mM DBO, 1.5 mM CB7, 25.0 mM Ag⁺. [d] Not determined due to overlap with solvent peak.

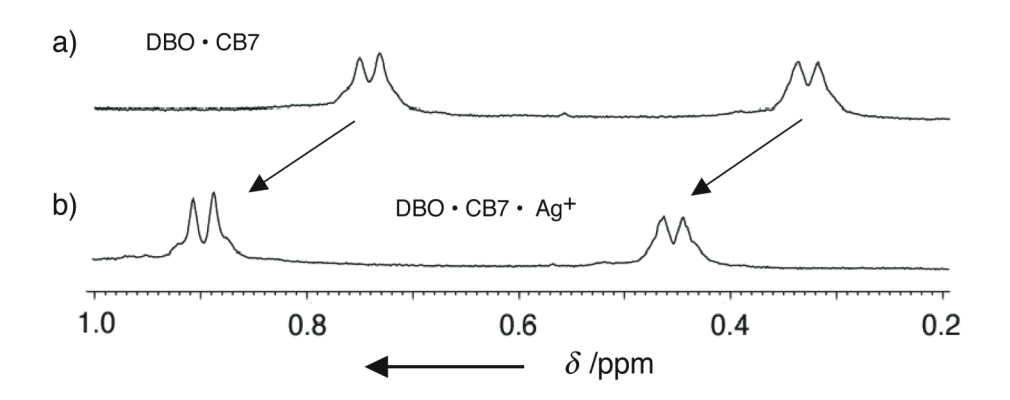


Figure S2. Chemical shifts of the ethano bridge protons of DBO (1.0 mM) a) in the presence of CB7 (1.5 mM, binary complex) and b) upon subsequent addition of Ag⁺ (25.0 mM, ternary complex).

Table S2. Complexation-induced chemical shifts of the DBH protons upon addition of CB7 (binary complex) and Ag⁺ (metal-ligand complex) and upon addition of both additives (ternary complex) in D₂O at pD 5.4

			δ/ppm			
System	H_{endo}	H_{exo}	H_{syn}	H_{anti}	H_b	$\Delta \delta_{ m avg}$
DBH	0.72	1.53	1.16	1.16	5.06	_
DBH •Ag ^{+ [a]}	0.82	1.64	1.27	1.27	5.16	+0.11
DBH•CB7 [b]	-0.09	0.63	0.20	0.28	[d]	-0.87
DBH•CB7•Ag ⁺ [c]	0.05	0.88	0.40	0.58	[d]	-0.65

[[]a] 2.0 mM DBH, 20.0 mM Ag⁺. [b] 2.0 mM DBH, 4.0 mM CB7. [c] 2.0 mM DBH, 4.0 mM CB7, 20.0 mM Ag⁺. [d] Not determined due to overlap with solvent peak.

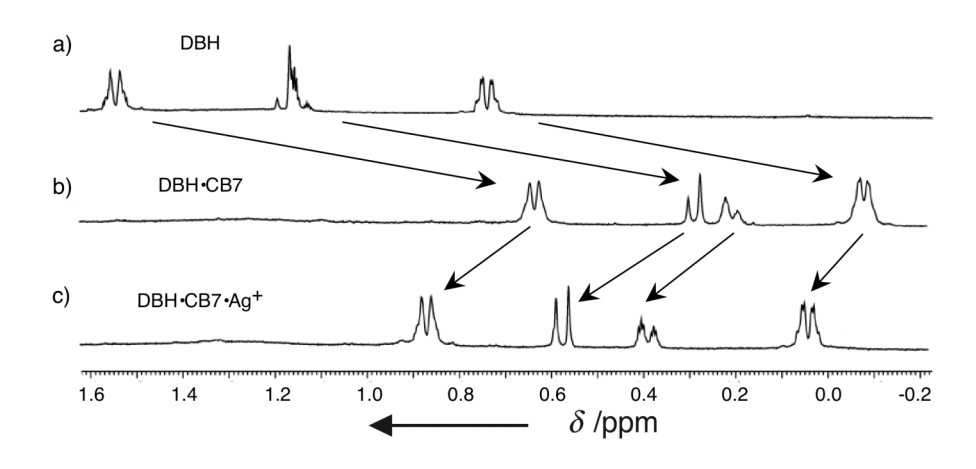


Figure S3. Chemical shifts of the bridge protons of DBH (2 mM) a) in the absence and b) in the presence of CB7 (4 mM, binary complex), and c) upon subsequent addition of Ag⁺ (20 mM, ternary complex) in D₂O at pD 5.4.

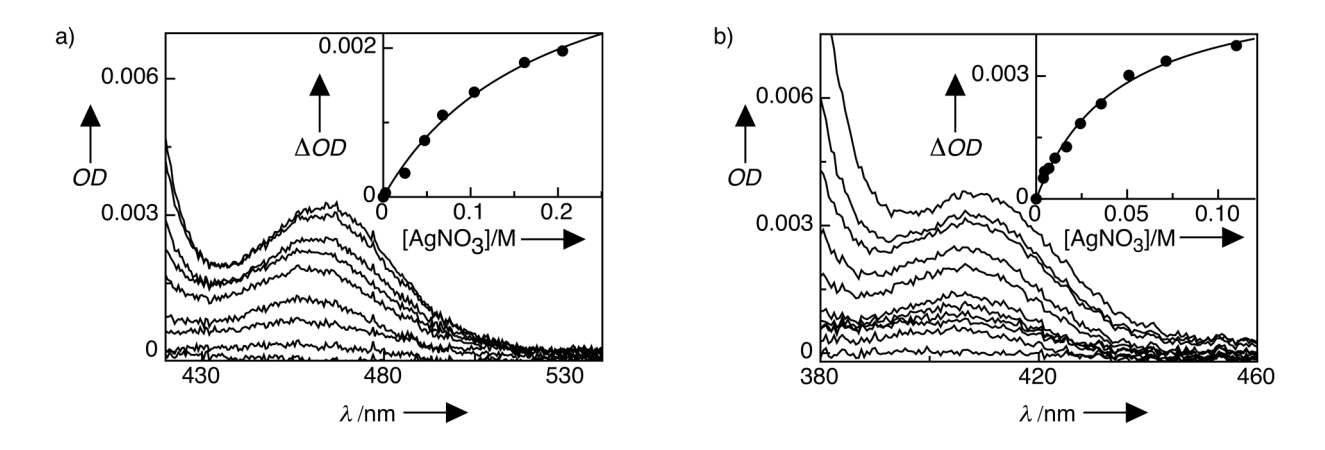


Figure S4. Variation of the charge-transfer bands in the UV-Vis spectra and corresponding titration plots (insets) of a) 1.0 mM DBO and b) 1.0 mM DBH upon addition of increasing amounts of Ag⁺ at pH 5.0. The data were fitted according to a 1:1 complexation model and provided the apparent binding constants of 10±5 M⁻¹ for DBO and 20±3 M⁻¹ for DBH.

Spectroscopic evidence for the formation of the ternary complexes

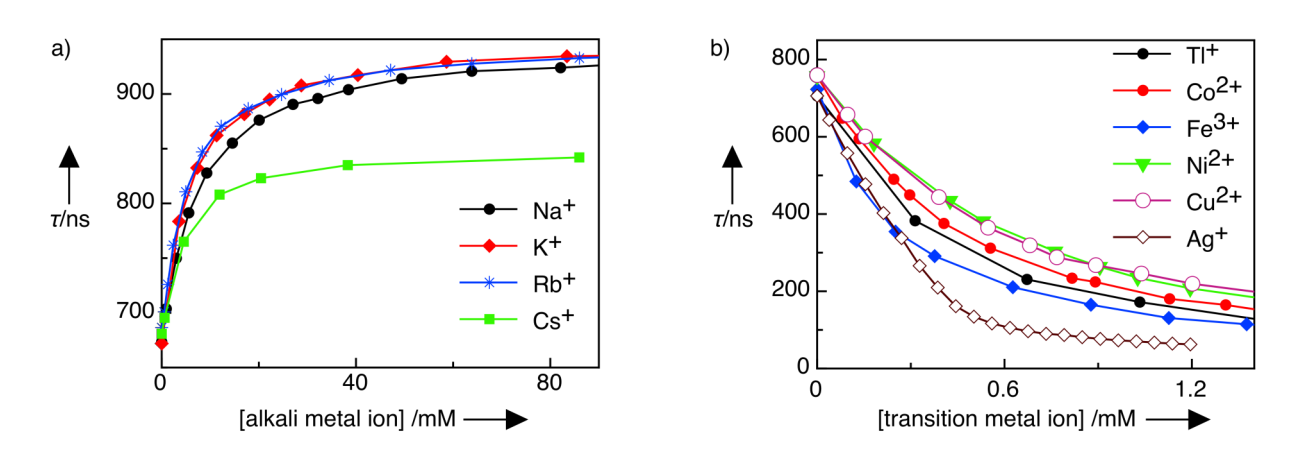
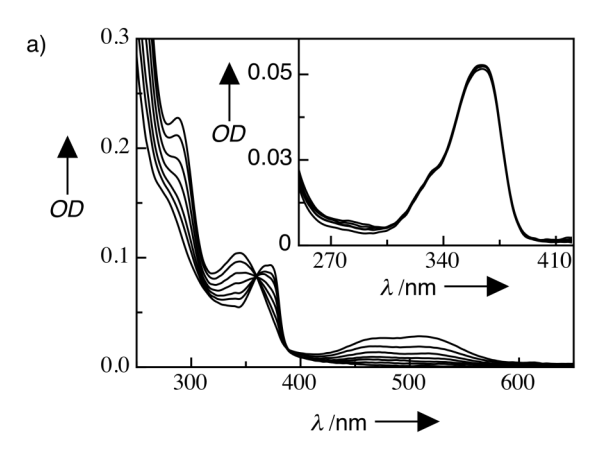


Figure S5. Effect of the successive addition of a) alkali and b) transition metal ions and TI^+ on the fluorescence lifetime of the DBO•CB7 complex (0.2 mM DBO and 0.3 mM CB7). The addition of the respective alkali salts to a solution only containing the free DBO chromophore has no significant effect on its fluorescence lifetime (325 \pm 10 ns). The addition of the respective transition metal salts to a solution only containing the free DBO chromophore causes also a (dynamic) fluorescence quenching, but much higher concentrations are required to reach comparable quenching effects.



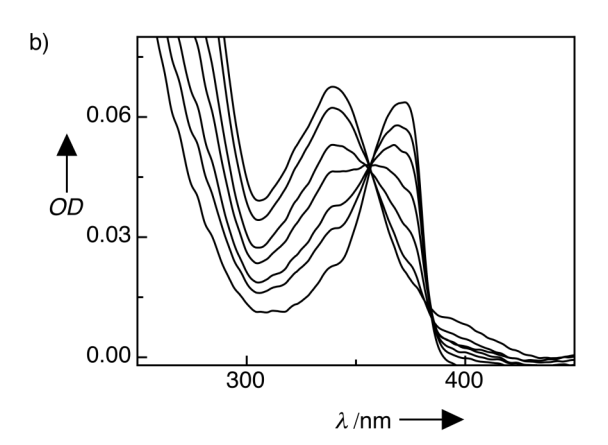
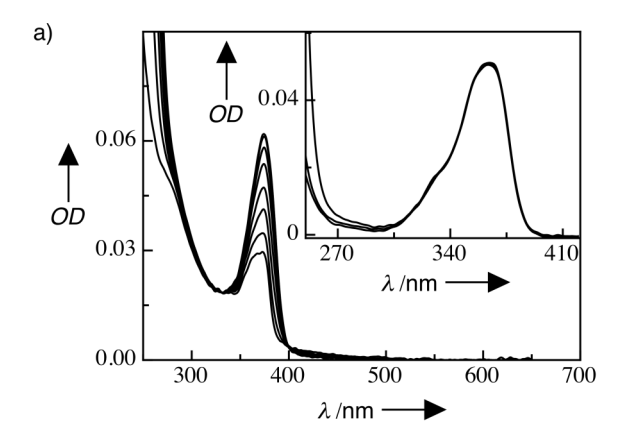


Figure S6. Changes in the UV absorption spectra of the pre-formed DBO•CB7 complex (1.5 equiv. CB7) upon successive addition of a) Co²⁺ (up to 5.0 mM) and b) Ni²⁺ (up to 5.0 mM). Note the hypsochromic shift of the absorption band of the azo chromophore near 350 nm, which is characteristic for the formation of a ternary complex in which the azo group functions as monodentate ligand. The inset shows the absence of a hypsochromic shift (and therefore the absence of the formation of a metal-ligand bond between DBO and Co²⁺) when the same titration is performed without CB7.



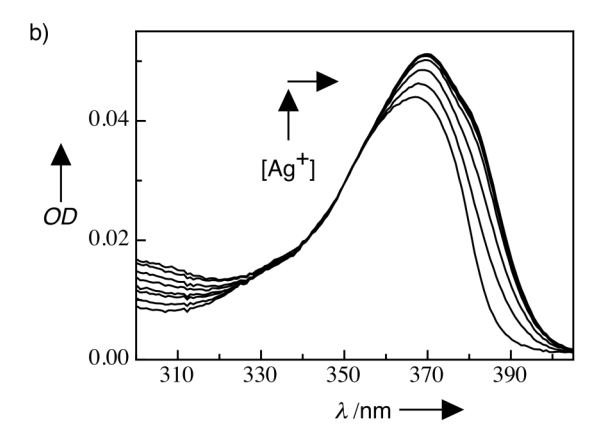


Figure S7. Changes in the UV absorption spectra of the pre-formed DBO•CB7 complex (2 equiv. CB7) upon successive addition of a) Tl⁺ (up to 2.5 mM) and b) Ag⁺ (up to 5.0 mM). Note the bathochromic (from 367 to 371 nm in b) and hyperchromic shift of the absorption band of the azo chromophore, which is characteristic for the formation of a ternary complex in which the azo group functions as a bidentate ligand. The inset in a) shows the absence of an effect on the absorption band (and therefore the absence of the formation of a metal-ligand bond between DBO and Tl⁺) when the same titration is performed without CB7.

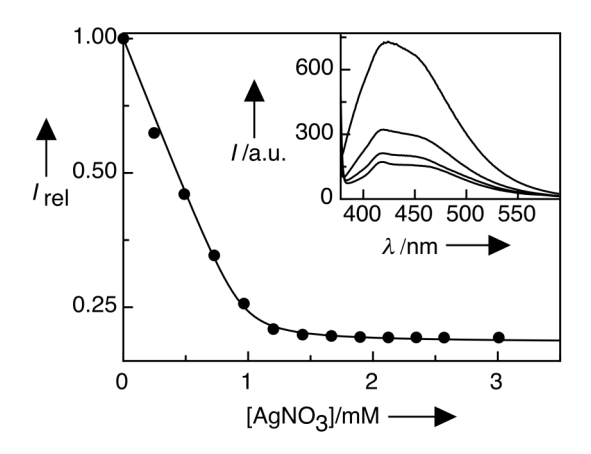


Figure S8. Steady-state fluorescence quenching of the pre-formed binary DBO•CB7 complex (1 mM DBO and 1.8 mM CB7) upon addition of Ag^+ and corresponding fluorescence titration curve fitted with a simple 1:1 complexation model, affording an apparent binding constant of $(6.0\pm1.8) \times 10^4 \text{ M}^{-1}$. Note that the fluorescence intensity (and also fluorescence lifetime, *cf*. Figure S5) reaches a plateau with nonvanishing magnitude (ca. 20% of the initial intensity), which confirms the formation of a new species (the ternary complex with finite fluorescence intensity and lifetime), and rules out a simple dynamic fluorescence quenching.

Single-crystal X-ray analysis. Single crystals of the silver complex were obtained by slow evaporation of the solvent from an aqueous solution containing 2 mM DBO, 4 mM CB7, and 10 mM AgNO₃. X-ray analysis was performed on a Bruker X8 APEX II CCD diffractometer with kappa geometry using MoK_a (λ = 0.71073Å) radiation at 173(2) K. Data integration, data reduction, structure solution, and refinement were performed with the SAINT Bruker software suite.^[9] Structures were solved by direct methods and completed by successive interpretation of synthesis Fourier maps, followed by full matrix least-squares refinement against F^2 . Hydrogen atoms were included in fixed, calculated positions and assigned a thermal parameter based on the bonded atom. The CIF file of the crystal structure has been deposited under the code CCDC 790262; these data can be obtained free of charge from The Cambridge Crystallographic Data Centre via www.ccdc.cam.ac.uk/data_request/cif.

Description of crystal structure. Formula $C_{48}H_{52}O_{21}N_{32.33}Ag_{2.33}$ •12 H_2O (corresponding to 3DBO•3CB7•7AgNO₃•36 H_2O for the asymmetric unit, $M_r = 1885.27$. The crystal was a colorless block with dimensions $0.33 \times 0.33 \times 0.25$ mm³, monoclinic, space group P_{21}/n , a = 21.162(3), b = 36.494(4), c = 30.374(4) Å, $\alpha = \gamma = 90^{\circ}$, $\beta = 102.515(5)^{\circ}$, V = 22900(5) Å³, Z = 12, $\rho_{cal} = 1.641$ Mg m⁻³, $\mu = 0.704$ mm⁻¹. $2\theta_{max} = 41.64^{\circ}$, measured reflections 353872, independent reflections 23910 ($R_{int} = 0.2382$). Carbon atoms, disordered oxygens and lattice waters were refined isotropically, other non-hydrogen atoms were refined anisotropically. The final anisotropic full matrix least-squares refinement on F^2 for 2767 variables converged at $R_1 = 0.1173$ and $wR_2 = 0.2885$ with a goodness-of-fit of 1.069. In the final difference map the largest peak was 3.529 e Å⁻³ and deepest hole -1.668 e Å⁻³. The refinement was limited by the supramolecular complexity of the structure and the disorder of the silver ions and associated water ligands.

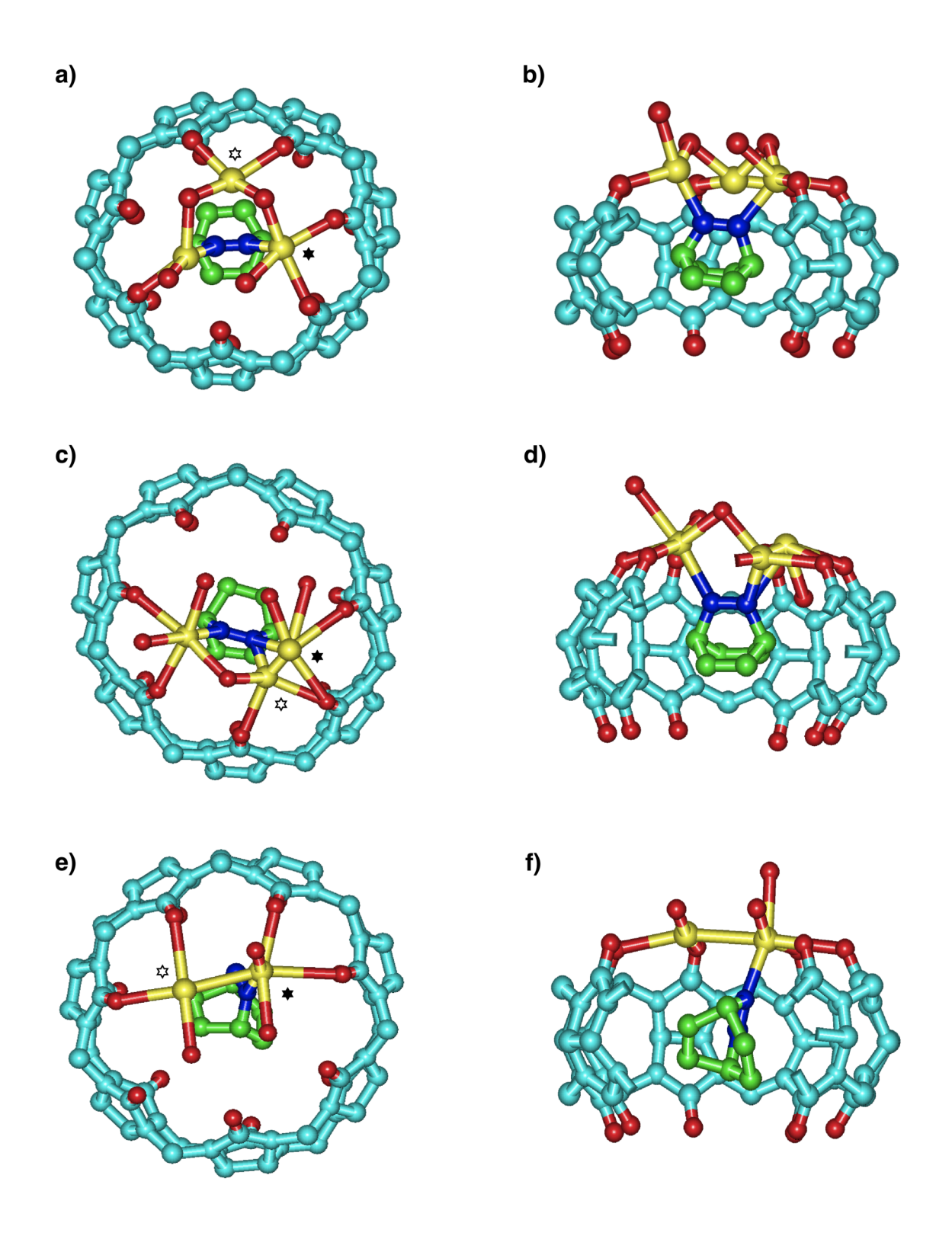


Figure S9. Crystal structure of the ternary complex between CB7, DBO, and silver ions showing the three distinct host-guest complexes in the asymmetric unit (magenta: cucurbituril skeleton, green: guest carbons, red: oxygens, blue: azoalkane nitrogens, yellow: silver ions). Each row corresponds to one complex viewed from the top (left) and dissected from the side (right). Disordered silver atoms are marked with filled (position with major occupancy) or open asterisks (minor occupancy).

The crystal structure presents one of the rare examples of a direct coordination of the carbonyl groups of a cucurbituril with a transition metal, [10] and the first one, to our knowledge, for CB7. The structure has three distinct host-guest complexes between CB7, silver ions, and DBO in the asymmetric unit. In each of the 4 asymmetric units of a unit cell are 7 silver ions and 3 CB7 molecules and each CB7 accommodates a DBO in its hydrophobic cavity. Two silver ions connect three CB7 molecules by forming coordinative bonds between the carbonyl groups of one (the "lower") CB7 portal. This presents the first example of a transition metal complexation which involves exclusively cucurbituril carbonyls as ligands. The remaining 5 silver ions are involved in coordinative bonds with the azo group of the included DBO at the second (the "upper") rim. 2 of 3 CB7 macrocycles of the asymmetric unit are capped with 2 silver ions at one portal (one of which disordered over two positions), and both coordinating with DBO and using the azo group as a bidentate ligand. The distance between the 2 silver ions simultaneously bound to the same cucurbituril rim is, however, too large (> 3.3 Å) to be assigned to a Ag-Ag bond.^[11] The remaining CB7 is only capped with a single silver ion (disordered over 2 positions) at the upper rim, also coordinating with DBO, but using the azo group as monodentate ligand.

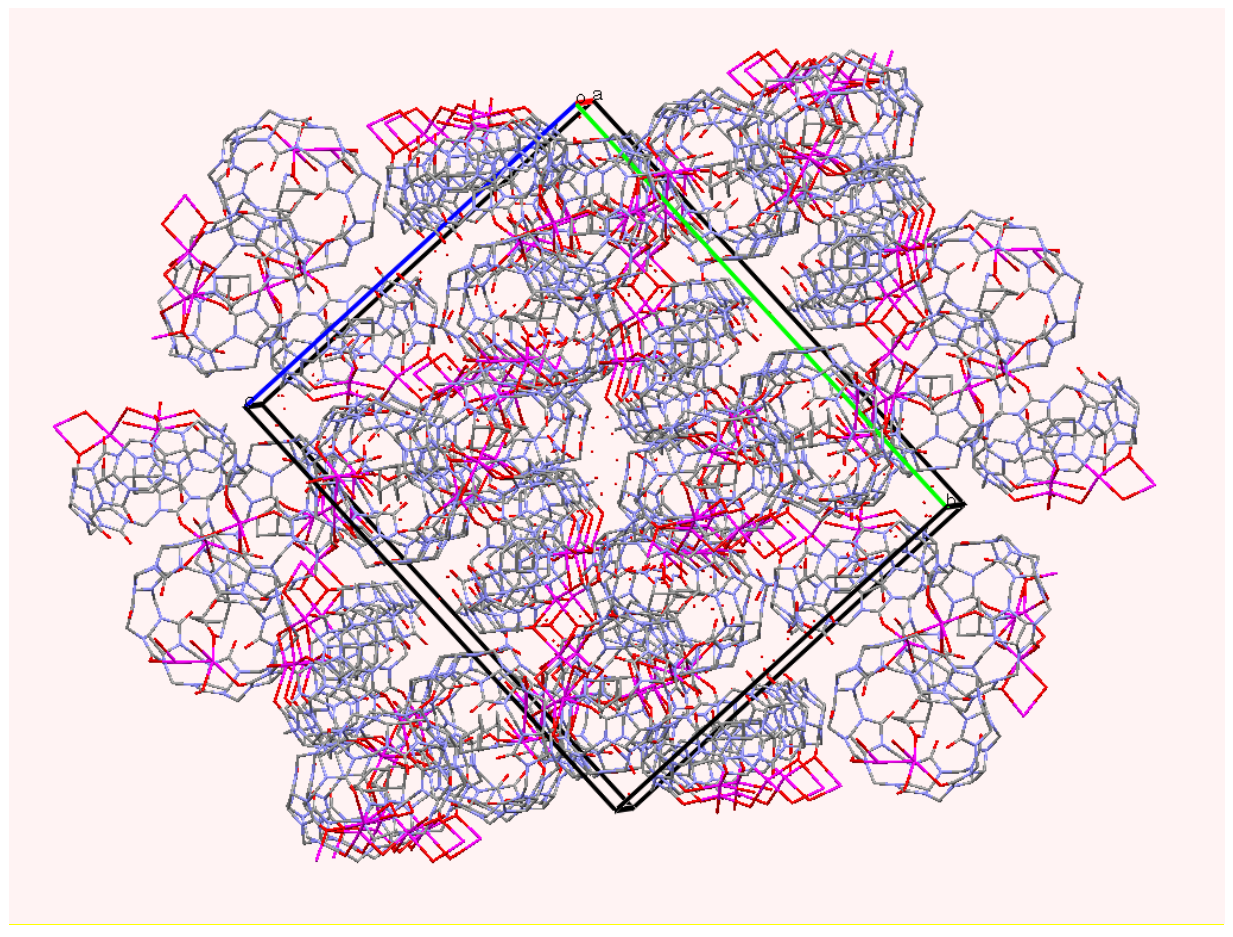


Figure S10. Packing diagram for the crystal structure, viewed along the a axis; C atoms are grey, N blue, O red, and Ag purple. Red dots represent solvent water molecules. All hydrogen atoms and counter anions (NO_3^-) are removed for clarity.

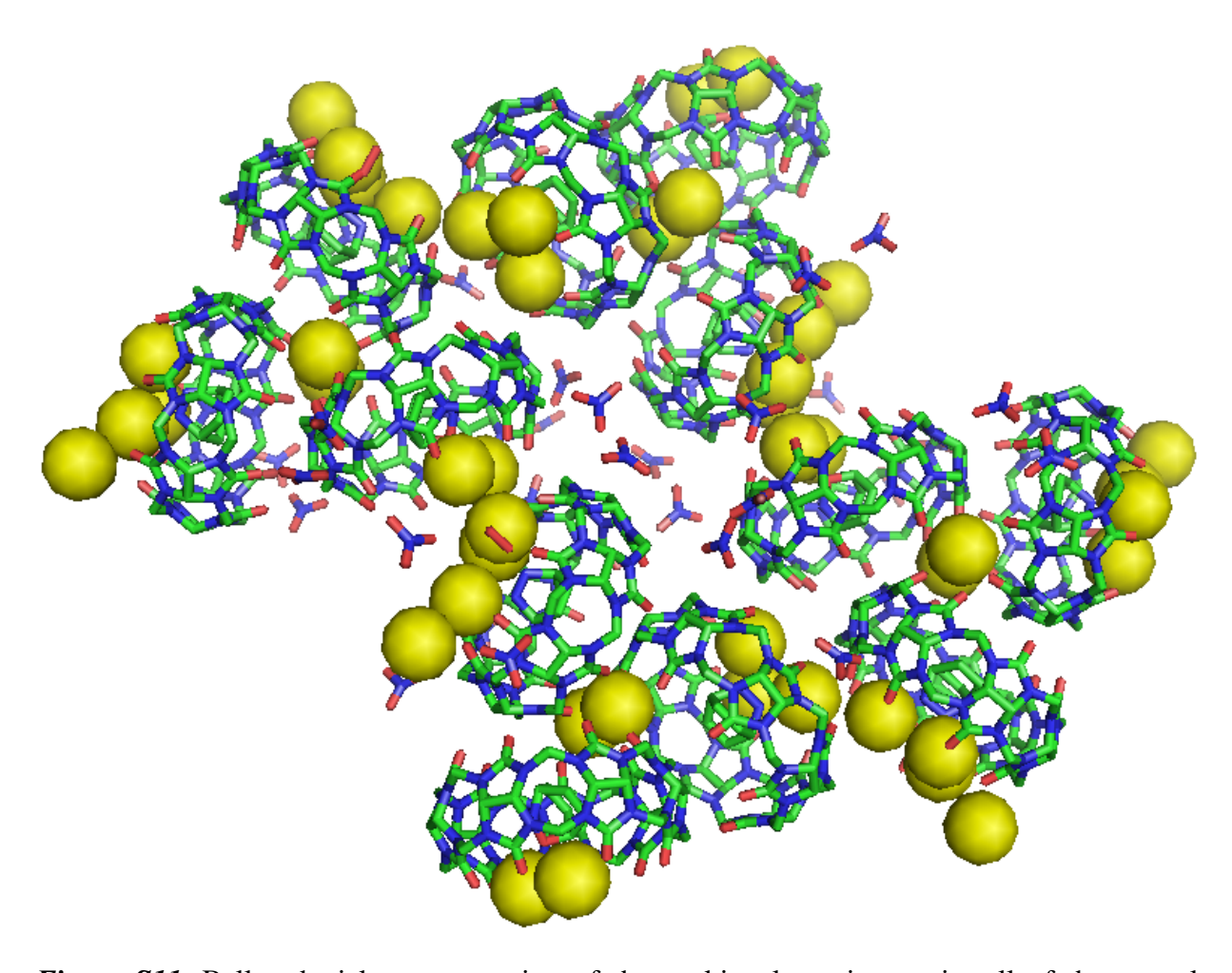


Figure S11. Ball-and-stick representation of the packing layer in a unit cell of the crystal structure. All silver ions are shown as yellow balls. The CB7 macrocycles and nitrate counter anions are represented as sticks. All hydrogens and water molecules are removed for clarity.

Binding constants and positive cooperativity for ternary complex formation

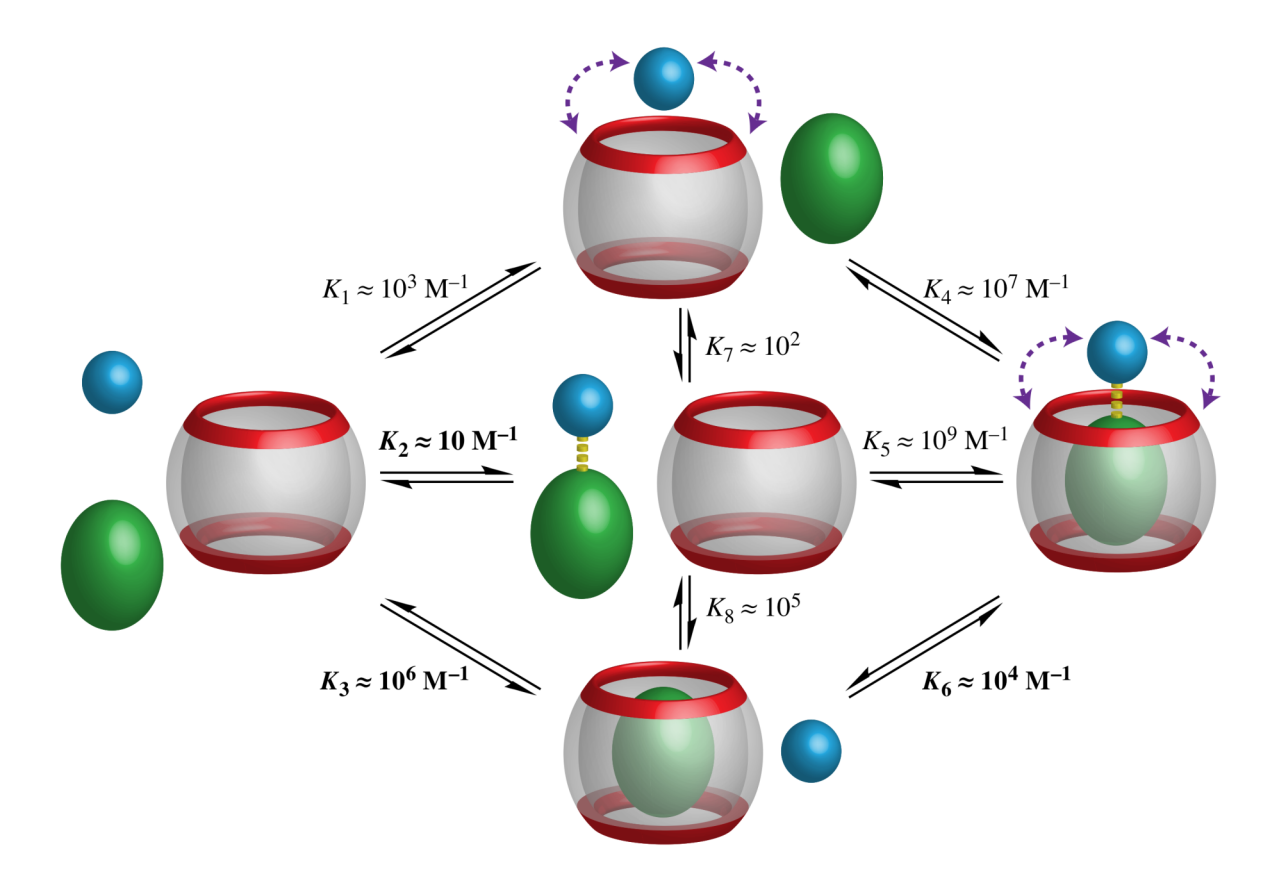


Figure S12. Binding constants (orders of magnitude estimates) for the formation of the different binary and ternary complexes as projected from the experimentally accessible (shown in bold) binding constants, i.e., K_2 from the titrations in Figure S4, K_3 from the titrations in Figure S1, and K_6 from the titrations in Figure S8; binding constant K_1 was estimated from reported binding constants of metal ions with CB6^[12,13] and CB7^[14] and can be independently obtained by assuming that ion-dipole attraction to the carbonyl rim and metal-ligand bond formation are independent supramolecular interactions (i.e., $K_1 = K_6/K_2$). The remaining binding constants follow from thermodynamic cycles. Note the positive cooperativity and template effect of CB7, i.e., the binding of the metal ion to the substrate is greatly increased by the presence of the host $(K_6 >> K_2)$, which provides the basis for the observed effects on the chemoselectivity of the photoreactions.

Photolyses. Steady-state photoreactions were carried out in a Luzchem LZC-4V photoreactor equipped with 14 Hitachi FL8BL-B UVA lamps ($\lambda_{max} = 350$ nm); for the determination of the photoproduct distributions, the photolyses were performed in GC vials containing 3 ml of an aqueous solution (adjusted to pH 5) and 0.5 ml organic solvent (n-pentane for DBO, toluene for DBH). 15-20 h irradiation time were selected for DBO, and 0.5-1.5 h for DBH and the photolyses were carried out without degassing (a control experiment revealed that the presence of oxygen did not affect the photoproduct distributions). The laser excitation was performed with the third harmonic (355 nm) of a Nd-YAG laser (Continuum Surelite III) by selectively irradiating the lower, aqueous phase of a cyclindrical long-necked cuvette containing ca. 3 ml

of aqueous solution in the cyclinder volume and ca. 0.5 ml of organic solvent in the neck, *cf.* Figure 3 in main text. After the addition of 15 mM cadaverine (a competitive guest for CB7 to displace any bound photoproducts)^[15] to the reaction mixture and shaking, aliquots were drawn from the organic phase for GC analysis of the photoproducts and distributions.

Table S3. Photoproducts of DBO under different conditions in the absence and presence of CB7 and/or metal ions^[a]

Host	Metal ion	HD ^[b]	BCH ^[b]
	^[c]	65	35
CB7		65	35
CB7	$\mathrm{Li}^{^{+}}$	68	32
CB7	Na ⁺	69	31
CB7	K^{+}	67	33
CB7	Rb^{+}	67	33
CB7	Cs^+	70	30
CB7	Mg^{2^+}	67	33
CB7	Ca ²⁺	72	28
CB7	Sr^{2+}	73	27
CB7	Ba^{2+}	74	26
CB7	Cr ³⁺	73	27
CB7	Mn^{2^+}	75	25
CB7	Fe^{3+}	87	13
CB7	Co ²⁺	88	12
CB7	Ni ²⁺	88	12
CB7	Cu ²⁺	85	15
CB7	Zn^{2+}	66	34
CB7	\mathbf{Ag}^{+}	90	10
CB7	Cd^{2+}	63	37
CB7	\mathbf{Tl}^{+}	83	17
CB7	Pb^{2+}	75	25
CB7	La^{3+}	68	32
CB7	Eu ³⁺	75	25

^[a] Concentrations were 2 mM DBO, 4 mM CB7, and 10 mM metal ion. ^[b] Products correspond to 1,5-hexadiene and bicyclo[2.2.0]hexane, see Eq. 1 in main text. ^[c] Same product distribution in D₂O, product distribution in *n*-pentane: 71% HD, 29% BCH.

Photoproduct distributions by GC analysis. GC measurements were performed with a Varian CP3800 gas chromatograph built in a Varian Saturn 2000 mass spectrometer. Gas chromatographs were measured by using an FID detector with a non-polar fused silica column (CP 8912, 30 m × 0.25 mm i.d., 0.25 m × 1.0 m thickness, and external diameter 0.39 mm). Photoproduct analysis of the DBO photolysate (Table 1 in main text and Table S-3) in n-pentane was performed according to the following temperature program: $T_{\rm inj} = 250$ °C, $T_{\rm dec} = 100$ °C, T_{\rm

280°C, starting temperature 30°C with a hold time of 3 min followed by an increase in the temperature up to 280°C with a rate of 30°C/min, and a hold time of 2 minutes at 280°C. The photoproducts of DBO, i.e., 1,5-hexadiene and bicyclo[2.2.0]hexane, were observed with a retention time of 3.77 and 4.82 minutes, respectively; the retention time of 1,5-hexadiene was verified with a standard sample.

Photoproduct analysis of the DBH photolysate (Table 2 in main text) in toluene was performed according to the following temperature program: $T_{\rm inj} = 250^{\circ}\text{C}$, $T_{\rm dec} = 280^{\circ}\text{C}$, starting temperature 30°C with a hold time of 3 min followed by an increase in the temperature up to 280°C with a rate of 9°C/min, and a hold time of 3 minutes at 280°C. The common photoproduct bicyclo[2.1.0]pentane and the new photoproduct cyclopentene were observed with a retention time of 3.15 and 3.28 minutes, respectively; the retention time of cyclopentene was again verified with a standard sample. The identity of the photoproduct cyclopentene was independently confirmed by NMR analysis. The error in the relative photoproduct yields from the GC measurements (reproducibility from independent photolyses as well as from repeated injections) was estimated as \pm 3%.

Control experiments. Extensive control experiments at different temperatures (without cooling in the photoreactor and cooled in ice), at lower pH (pH 3), and at prolonged irradiation times (40 instead of 20 h) were performed to exclude that local heating effects, slight variations of the pH, or secondary photolyses in the presence of the different salts were responsible for the observed variations of the photoproduct distributions. In addition, the photoproducts were obtained separately in the two-phase system and subsequently (after 90 min) resubmitted to metal ions as well as CB7 and metal ions. The photoproduct distribution remained, however, unchanged within error, which excludes that thermal follow-up reactions, particularly (Lewis) acid-catalyzed thermal ring opening, occurred under the reaction conditions. It should be mentioned that housanes can be ring-opened in both very strong acid (70% HClO₄, hot neat acetic acid) as well as by silver ions, [16-19] but the silver-catalyzed reaction depends critically on the presence of bridgehead alkyl or aryl groups to allow a tertiary or benzylic stabilization of the incipient cationic site during thermal ring opening. [16,18,19]

Calculations of the Gibbs energy of (photoinduced) electron transfer. The feasibility of photoinduced electron transfer from singlet-excited DBH to the silver ions coordinated to the cucurbituril rim according to Eq. 1 was evaluated according to Eq. S2 by considering free (uncomplexed) DBH and Ag⁺ ions as active donor and acceptor species, respectively (the Coulombic work term was omitted since one of the species in both reactants and products is uncharged).

$$\frac{1}{1} = \frac{1}{355 \text{ nm}} = \frac{1}{1} \left[\frac{N}{N} \right]^{*} + \frac{Ag^{+} Ag^{0}}{\Delta G_{PET}} \left[\frac{N}{N} \right]^{+} + \frac{-N_{2}}{1,2 \text{ H shift}} \right] + \frac{Ag^{0} Ag^{+}}{\Delta G_{BET}} (S1)$$

$$\triangle G_{\text{ET}}/(\text{KJmol}^{-1}) = 96.5[E^0(\text{Donor})/\text{V} - E^0(\text{Acceptor})/\text{V} - E^*(\text{Donor})/\text{eV}]$$
 (S2)

Taking $E^0(DBH^{*+}/DBH) = +1.97 \text{ V}$ vs SCE, $E^{[20]}$ $E^0(Ag^+/Ag^0) = +0.56 \text{ V}$ vs SCE, and $E^*(DBH) = +3.66 \text{ eV}$, $E^{[21]}$ one obtains a very strongly exergonic value of $\Delta G_{PET} = -217 \text{ KJmol}^{-1}$. The back electron transfer process after 1,2-H shift (oxidation of $E^0(S)$ by the cyclopentene radical cation, see $E^0(S)$ is calculated with $E^0(S)$ cyclopentene radical cation/cyclopentene $E^0(S)$ vs $E^0(S)$ to be also strongly exergonic, with a value of $E^0(S)$ to be also strongly exergonic, with a value of $E^0(S)$ to be also strongly exergonic, with a value of $E^0(S)$ to be also strongly exergonic, with a value of $E^0(S)$ to be also strongly exergonic, with a value of $E^0(S)$ to be also strongly exergonic, with a value of $E^0(S)$ to be also strongly exergonic, with a value of $E^0(S)$ to be also strongly exergonic, with a value of $E^0(S)$ to be also strongly exergonic, with a value of $E^0(S)$ to be also strongly exergonic, with a value of $E^0(S)$ to be also strongly exergonic, with a value of $E^0(S)$ to be also strongly exergonic, with a value of $E^0(S)$ to be also strongly exergonic or the formation of silver in clusters.

Note that the reaction sequence in Eq. S1 would also be thermodynamically feasible for other one-electron oxidants, particularly Fe³⁺, but also or Cu²⁺. The fact that cyclopentene is not formed with these metal ions maybe due to the structure of the complexes (note that silver is one of the few metal ions that forms coordinative bonds with the carbonyls of cucurbiturils, *cf.* Description of Crystal Structure) and due to subtle thermodynamic variations. We speculate that electron transfer involving Fe³⁺ or Cu²⁺ would bring along a Coulombic penalty due to the formation of identical adjacent charges after forward electron transfer (Fe²⁺---DBH^{*+} or Cu⁺---DBH^{*+}), which could, among others, greatly accelerate back electron transfer from the DBH radical cation before it eliminates nitrogen.

Table S4. Photodecomposition quantum yields (ϕ_d) of DBO (2 mM) in different solvents and in the presence of CB7 and metal salts.

Solvent ^[a]	Host ^[b]	Metal ion ^[c]	$\varepsilon^{351 \text{ nm}}/(\text{M}^{-1}\text{cm}^{-1})$	Slope/10 ⁻³	$\phi_{\rm d}/10^{-3}$
H ₂ O			40	0.88	1.9
$H_2O^{[d]}$			40	1.03	2.2
$\mathrm{D_2O}^{[\mathrm{d}]}$			40	1.40	$3.0^{[e]}$
Benzene ^[d]			52	9.36	$15^{[f]}$
$H_2O^{[d]}$	β -CD ^[g]		35	2.06	$5.0^{[h]}$
$H_2O^{[d]}$	$CX4^{[i]}$		61	0.09	0.13
H_2O	CB7		31	3.99	11
H ₂ O/ <i>n</i> -pentane ^[j]	CB7		31	3.23	8.9
H_2O/n -pentane ^[j]	CB7	Cs^+	31	2.93	8.1
H ₂ O/ <i>n</i> -pentane ^[j]	CB7	Ba^{2+}	31	2.55	7.1
H_2O/n -pentane ^[j]	CB7	Zn^{2+}	33	2.68	7.0
H_2O/n -pentane ^[j]	CB7	Cu^+	40	1.25	2.7
H ₂ O/ <i>n</i> -pentane ^[j]	CB7	Co^{2+}	37	0.12	0.28

^[a] In aerated solution unless stated differently. ^[b] 4 mM unless stated differently. ^[c] 10 mM. ^[d] In deaerated solution (purged with nitrogen for 15 minutes). ^[e] From ref. ^[23], used as reference. ^[f] Lit.: ^[24,25] 11 × 10⁻³ at 21.9°C. ^[g] 6.5 mM. ^[h] Lit. ^[23]: ca. 3 × 10⁻³, in D₂O with 4 mM DBO and 16 mM β-CD. ^[i] 15 mM. ^[j] With *n*-pentane as upper phase.

Photodecomposition quantum yields of DBO. Photodecomposition quantum yields of DBO (2.0 mM) were determined in different solvents (ca. 3 mL), and in water in the presence of CB7 and metal ions by UV spectrophotometry (steady-state irradiation, see Photolyses). The quantum yield of decomposition of DBO in deaerated D_2O (0.3%) and its extinction coefficient ($\varepsilon^{351 \text{ nm}} = 40 \text{ M}^{-1} \text{ cm}^{-1}$) served as reference. The decay of the absorbance (A) at the absorption maximum ($A_0 \approx 0.1$) was monitored as a function of incident irradiation time. Plots of $\log([10^{4o}-1]/[10^4-1])$ versus irradiation time [21] were linear up to ca. 80% conversion of DBO. The ratio of the slopes of the logarithmic plots [after correction for the known extinction coefficients of DBO in the different solvents and complexes (see Figures S6 and S7)] provided the desired quantum yields.

The experimentally determined quantum yields of decomposition of DBO are listed in Table S4. The photodeazetation quantum yields in hydrophobic environments (benzene solution, β -CD inclusion complex, CB7 inclusion complex) are higher than those in aqueous solution, with the exception of the CX4 inclusion complex, which is known to act as a quencher of DBO, [3,26,27] Expectedly, alkali as well as redox-inactive transition metal ions (Zn²⁺) caused no large effect on the quantum yield, but redox-active transition metal ions caused a drop in photodecomposition quantum yield. This is expected, because transition metals cause (chemically frequently unproductive) quenching of excited states by a variety of mechanisms, including electron and energy transfer, but also enhanced intersystem crossing, in particular for paramagnetic metal ions. The photodecomposition quantum yields remained, nevertheless, sizable compared to the values in water.

Photodecomposition quantum yields of DBH. Owing to the very high values, photodecomposition quantum yields of DBH (2.0 mM) were estimated from the time to get comparable conversion by GC analysis (these reactions were performed under air with *n*-pentane as upper phase). The photolyses of DBH in toluene, water, and in presence of CB7 (4 mM) were all complete within 20 minutes, which suggested that the known unit quantum yield of DBH in organic solvents^[28] is transferable to both water and the CB7 inclusion complex. In the case of the ternary complex with Ag⁺ (30 mM) complete conversion was achieved in ca. 90 minutes, indicating a drop in quantum yield to ca. 20%. While this drop may not be desirable from the viewpoint of reaction efficiency, it provides compelling evidence for a direct photophysical interaction between singlet-excited DBH and Ag⁺, which is a prerequisite for the postulated reaction mechanism.

Mass balance determinations. The exceptionally high volatility of the photoproducts, particularly in the DBH photolyses, required special attention in all experiments, and mass balances were determined by ¹H NMR to ensure that the largest fraction of photoproducts could indeed be extracted. For this purpose, DBH solutions were quantitatively photolyzed (in a photoreactor, see Photolyses, and followed by UV) in D₂O as aqueous phase and with deuterated benzene as upper phase containing 1,4-dimethoxybenzene as internal standard in a GC vial. In the presence of CB7, cadaverine (15 mM) was added after the photoreaction to displace any photoproducts bound to the macrocycle before NMR analysis. The photolysis of 2 mM DBH in toluene could be performed with a mass balance of 87%, that in D₂O with one of

67%, that in D_2O with 4 mM CB7 with one of 88%, and that in D_2O with 4 mM CB7 and 30 mM AgNO₃ with 66%, confirming that the major fraction of the extremely volatile photoproducts could be recovered.

References

- [1] S. G. Cohen, R. Zand, C. Steel, J. Am. Chem. Soc. 1961, 83, 2895-2900.
- [2] R. Askani, Chem. Ber. 1965, 98, 2551-2555.
- [3] H. Bakirci, A. L. Koner, M. H. Dickman, U. Kortz, W. M. Nau, *Angew. Chem.* **2006**, 118, 7560-7564; *Angew. Chem. Int. Ed.* **2005**, 45, 7400-7404.
- [4] H. Bakirci, A. L. Koner, W. M. Nau, J. Org. Chem. 2005, 70, 9960-9966.
- [5] X. Zhang, G. Gramlich, X. Wang, W. M. Nau, J. Am. Chem. Soc. 2002, 124, 254-263.
- [6] J. Kim, I.-S. Jung, S.-Y. Kim, E. Lee, J.-K. Kang, S. Sakamoto, K. Yamaguchi, K. Kim, J. Am. Chem. Soc. 2000, 122, 540-541.
- [7] A. Day, A. P. Arnold, R. J. Blanch, B. Snushall, J. Org. Chem. 2001, 66, 8094-8100.
- [8] C. Márquez, F. Huang, W. M. Nau, *IEEE Trans. Nanobiosci.* 2004, 3, 39-45.
- [9] G. M. Sheldrick, Acta Cryst. 2008, A64, 112-122.
- [10] O. A. Gerasko, E. A. Mainicheva, M. I. Naumova, M. Neumaier, M. M. Kappes, S. Lebedkin, D. Fenske, V. P. Fedin, *Inorg. Chem.* **2008**, *47*, 8869-8880.
- [11] D. R. Whitcomb, M. Rajeswaran, Acta. Cryst. 2006, E62, m272-m274.
- [12] C. Márquez, R. R. Hudgins, W. M. Nau, J. Am. Chem. Soc. 2004, 126, 5806-5816.
- [13] H.-J. Buschmann, E. Cleve, L. Mutihac, E. Schollmeyer, *J. Incl. Phenom. Macro. Chem.* **2009**, *65*, 293-297.
- [14] M. Megyesi, L. Biczok, I. Jablonkai, J. Phys. Chem. C 2008, 112, 3410-3416.
- [15] Without the addition of cadaverine, slightly different product distributions in the DBO photolysis, and a significantly lower yield of cyclopentene (26% *versus* 41%) in the DBH photolysis, were obtained.
- [16] L. A. Paquette, L. M. Leichter, J. Am. Chem. Soc. 1972, 94, 3653-3655.
- [17] K. B. Wiberg, S. R. Kass, K. C. Bishop, J. Am. Chem. Soc. 1985, 107, 996-1002.
- [18] W. Adam, T. Heidenfelder, J. Am. Chem. Soc. 1998, 120, 11858-11863.
- [19] W. Adam, C. P. Librera, F.-G. Klärner, F. Wurche, J. Am. Chem. Soc. 2003, 125, 995-1001
- [20] W. M. Nau, W. Adam, D. Klapstein, C. Sahin, H. Walter, J. Org. Chem. 1997, 62, 5128-5132.
- [21] W. Adam, G. Fragale, D. Klapstein, W. M. Nau, J. Wirz, J. Am. Chem. Soc. 1995, 117, 12578-12592.
- [22] P. G. Gassman, R. Yamaguchi, G. F. Koser, J. Org. Chem. 1978, 43, 4392-4393.
- [23] W. M. Nau, X. Zhang, J. Am. Chem. Soc. 1999, 121, 8022-8032.
- [24] G. Greiner, M. Feth, H. Rau, W. M. Nau, J. Inf. Recording 1998, 24, 115-122.
- [25] P. S. Engel, C. J. Nalepa, L. R. Soltero, D. W. Horsey, D. E. Keys, *J. Am. Chem. Soc.* **1983**, *105*, 7108-7114.
- [26] H. Bakirci, W. M. Nau, Adv. Funct. Mater. 2006, 16, 237-242.
- [27] The efficient quenching caused by CX4 was also the reason why we could not conduct comparable photoreactions with metalloenzyme models composed of DBO, CX4, and transition metal ions, which assemble to form structurally related, but nonfunctional ternary complexes, *cf.* ref. 3)
- [28] P. S. Engel, Chem. Rev. 1980, 80, 99-150.